

This article was downloaded by:

On: 14 January 2011

Access details: *Access Details: Free Access*

Publisher *Taylor & Francis*

Informa Ltd Registered in England and Wales Registered Number: 1072954 Registered office: Mortimer House, 37-41 Mortimer Street, London W1T 3JH, UK



## **Molecular Simulation**

Publication details, including instructions for authors and subscription information:

<http://www.informaworld.com/smpp/title~content=t713644482>

### **Molecular dynamics simulations of valveless pumping in a closed microfluidic tube-system**

J. S. Hansen<sup>a</sup>; J. T. Ottesen<sup>b</sup>; A. Lemarchand<sup>a</sup>

<sup>a</sup> Laboratoire de Physique Théorique de la Matière Condensée, Université Pierre et Marie Curie, Paris Cedex 05, France <sup>b</sup> Department of Mathematics and Physics, Roskilde University, Roskilde, Denmark

**To cite this Article** Hansen, J. S. , Ottesen, J. T. and Lemarchand, A.(2005) 'Molecular dynamics simulations of valveless pumping in a closed microfluidic tube-system', *Molecular Simulation*, 31: 14, 963 — 969

**To link to this Article:** DOI: 10.1080/08927020500419297

**URL:** <http://dx.doi.org/10.1080/08927020500419297>

PLEASE SCROLL DOWN FOR ARTICLE

Full terms and conditions of use: <http://www.informaworld.com/terms-and-conditions-of-access.pdf>

This article may be used for research, teaching and private study purposes. Any substantial or systematic reproduction, re-distribution, re-selling, loan or sub-licensing, systematic supply or distribution in any form to anyone is expressly forbidden.

The publisher does not give any warranty express or implied or make any representation that the contents will be complete or accurate or up to date. The accuracy of any instructions, formulae and drug doses should be independently verified with primary sources. The publisher shall not be liable for any loss, actions, claims, proceedings, demand or costs or damages whatsoever or howsoever caused arising directly or indirectly in connection with or arising out of the use of this material.

# Molecular dynamics simulations of valveless pumping in a closed microfluidic tube-system

J.S. HANSEN<sup>†\*</sup>, J.T. OTTESEN<sup>‡</sup> and A. LEMARCHAND<sup>†</sup>

<sup>†</sup>Laboratoire de Physique Théorique de la Matière Condensée, Université Pierre et Marie Curie, C.N.R.S. U.M.R. 7600, 4, place Jussieu, 75252 Paris Cedex 05, France

<sup>‡</sup>Department of Mathematics and Physics, Roskilde University, P.O. Box 260, 4000 Roskilde, Denmark

(Received September 2005; in final form October 2005)

In this paper, we study the flow which is generated by a valveless pumping mechanism in a closed micro-fluidic tube-system consisting of two tubes with different radii. This system has been investigated by Ottesen [J. T. Ottesen, *J. Math. Biol.* **46**, 309, (2003)] at a macroscopic level. We find that the results from the microscopic simulations qualitatively agree with the macroscopic results. Especially, it is shown that the direction of the flow changes with changing pumping frequency and the location of the pumping device. We study the local flow generated in the system and show that the stream velocities away from the pumping area can be modeled by a superposition of a plug flow and a zero-mean oscillatory flow.

**Keywords:** Valveless pumping; Nonequilibrium molecular dynamics; Moment current; Stream velocity; Oscillatory flow

## 1. Introduction

In the last decade, phenomena on very small time and length scales have drawn the attention of the research community and new disciplines, like synthesis of nanomaterials, nanofluidics and nanotechnology, have emerged. Currently, microscopic devices such as miniaturised heat exchanges that cool integrated circuits, micro-chemical reactors in which hazardous materials are produced, lap-on-a-chip and biochemical sensors are being developed [1–3]. For all these systems very small volumes of fluid are moving through the components. It is, therefore, of great importance to develop microscopic pumping devices, which can transport the fluid. Traditionally, the pumping devices have been composed of valves, peristaltic moving walls, nozzles, etc. [4]. However, such mechanic components are not easily manufactured on very small scales and it is, therefore, desirable to find an alternative.

Ottesen has recently proposed a very simple pumping mechanism which can be applied to closed tube-systems [5,6]. The system consists of two rubber tubes with same length, but different radii and elasticities. The two tubes are connected at both ends and form a closed torus. If the torus is filled with a liquid, e.g. water, and if one of the tubes is symmetrically and periodically compressed (for example

by a mechanical finger) at a point of asymmetry on the torus, i.e. not in the middle of the tube, a mean flow is generated in the system. A remarkable feature of this system is that the direction of the mean flow is changed by simply changing the pumping frequency or the pressure point. This pumping device overcomes many technical difficulties present in the production of traditional pumping components. Since no valve is needed, the mechanism is referred to as valveless pumping.

Previously this pumping mechanism has been applied and studied at a macroscopic level, i.e. at a length scale of the order of centimeters and time scale of the order of seconds [5]. As it has been shown in numerous studies are the fluid mechanisms not the same at a microscopic scale, see for example [7–10]. In narrow channels the velocity adjacent to the wall is characterised by a very large variation indicating an abnormal decrease in viscosity [11,12]. Furthermore, molecular dynamics studies of flows of Lennard–Jones fluids in carbon nanotubes show large velocity slip at the wall–fluid boundary [13,14]. It is therefore not obvious that the pumping mechanism can be applied to microscopic systems.

Ottesen [5,6] has proposed a model for the pumping mechanism based on the assumption that the velocity can be described by one-parameter velocity profiles. While this choice reduces the parameter space considerably and

\*Corresponding author. Email: schmidt@zigzak.net

can account for the physical experiments, it probably does not offer a correct description of the real physics. If molecular dynamics can capture the features of the pumping mechanism, it will provide a valuable tool for investigating the underlying fluid dynamics. The purpose of this paper is therefore twofold: first, we investigate whether the remarkable phenomena seen in the valveless pumping mechanism can be captured at much smaller time and length scales. Then we wish to study the fluid dynamics of the system and propose a more detailed model for the velocity profile. To do so, we use nonequilibrium molecular dynamics (NEMD) where the length scale is of the order  $10^{-7}$  m and the overall simulation time is of the order of  $10^{-8}$  s.

The next section describes how the tube-system is implemented and how the pumping device is modeled in the molecular dynamics simulations. In section 3, we present the results from the simulations and in section 4 we shall use these results to derive a model for local velocity profile. In the last section, we will make a final conclusions and give a few perspective remarks.

## 2. Molecular dynamics

We study fluid particles embedded in a two-dimensional domain which interact through the cut and shifted Lennard–Jones potential:

$$\phi(r_{ij}) = \begin{cases} 4\epsilon \left[ \left( \frac{\sigma}{r_{ij}} \right) - \left( \frac{\sigma}{r_{ij}} \right)^6 \right] - \phi(r_c) & \text{if } r_{ij} \leq r_c \\ 0 & \text{otherwise} \end{cases}$$

where  $\sigma$  and  $\epsilon$  define a length scale and interaction strength, respectively, and  $r_c$  is the cutoff radius which is set to  $2^{1/6}\sigma$  [15,16]. This type of potential is often referred to as the Weeks–Chandler–Anderson (WCA) potential. Any physical parameter can now be expressed in appropriate units of  $\sigma$ ,  $\epsilon$  and particle mass  $m$ . Here, we will omit writing the physical units explicitly and simply apply the reduced dimensionless quantities. According to work of Delhommelle and Evans [12] and Travis *et al.* [8] we will consider the tube walls as being a framework of atoms initially arranged on a triangle lattice and with number density fixed at 0.90. The atom is kept in place around its equilibrium (initial) position by a restoring spring force  $\mathbf{F}(\mathbf{r}) = -k(\mathbf{r}_{\text{eq}} - \mathbf{r})$  where  $k = 150.15$  is the spring constant,  $\mathbf{r}$  is the atom position and  $\mathbf{r}_{\text{eq}}$  is the equilibrium position. The wall atoms interact with the fluid particles and the neighboring wall atoms through the Lennard–Jones potential described above but with cutoff radius of  $r_c = 2.5$ . In this way, the wall–fluid interaction has an attractive radius whereas the fluid–fluid interaction is purely repulsive and we thereby include a “wetting” effect minimizing the adhesive slip at the wall–fluid boundary. The tube consists of four layers of wall atoms. For a smaller number of layers we have observed that the fluid particles may escape the tube in the pumping

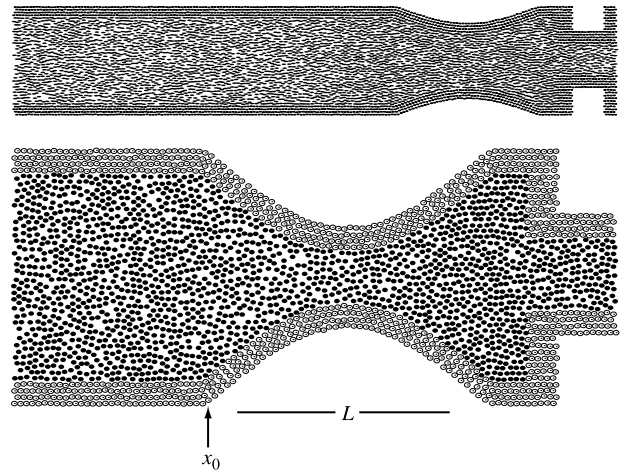


Figure 1. Two snap shots of the simulation box. The white dotted circles represent the wall atoms and the filled black circles represent the fluid particles. Upper figure shows the hole tube system. Lower figure shows the pumping area at maximum compression. See text for further details.

area. In the last tenth part of the hole tube the wall is located such that there will exist a narrowing with half the width, see figure 1. By letting the length of the narrow channel be only one tenth of the hole tube we minimise the density variations generated by the pumping mechanism.

To simulate the pumping mechanism we let the equilibrium position,  $\mathbf{r}_{\text{eq}}$ , of a wall atom move in an oscillatory manner if it is located in the pumping area. Specifically, we only move the  $y$ -component of  $\mathbf{r}_{\text{eq}} = (r_{\text{eq},x}, r_{\text{eq},y})$  according to:

$$r_{\text{eq},y}(t, x) = A \sin(\pi(x - x_0)/L) \sin(\omega t) \quad (1)$$

where  $A$  is the amplitude,  $x_0$  is the position where the pumping area starts,  $L$  is the length of the pumping area and  $\omega$  is the angular pumping frequency. If the wall atom is located in the upper wall  $A$  is negative, and vice versa, if the wall atom is located in the lower wall  $A$  is positive. The amplitude  $A$  is chosen such that the tube is not completely obstructed since this will increase the fluid density too much. The lower figure in figure 1 shows the tube at maximum compression. We believe this compression may be achieved in real physical experiments by an artificial muscle based on polymers hydrogel [17].

In order to keep the mean kinetic temperature constant, the wall atoms are coupled to a Nosé–Hoover thermostat [18–20], such that the heat generated in the viscous fluid is removed by heat conduction at the wall–fluid boundary. In the simulations the mean temperature of the fluid is kept in the range  $1.22 < T < 1.55$ . It should be noted that the heat generated depends on the pumping frequency and we therefore let the wall temperature vary with frequency. Using periodic boundary conditions in the  $x$ -direction we simulate a closed connected tube system. The fluid particles are integrated forward in time using the leap-frog integration scheme. Both the leap-frog scheme and Nosé–Hoover thermostat use a time step of  $dt = 0.005$ , the systems dimension is  $L_x \times L_y = 210 \times 42$  and the fluid density is set to 0.6.

### 3. Simulation results

The direction of the fluid flow is determined by monitoring the momentum current which is defined as the sample average of the moments of the fluid particles:

$$\mathbf{p}(t) = \frac{1}{N} \sum_{i=1}^N m_i \mathbf{v}_i(t)$$

where  $\mathbf{v}_i(t)$  is the velocity of particle  $i$  at time  $t$ . Since we apply periodic boundaries in the  $x$ -direction we are interested in the  $x$ -component of the momentum current,  $p_x(t)$ . The mean momentum current in the  $x$ -direction then follows as:

$$\bar{p}_x = \frac{1}{t'} \int_0^{t'} p_x(t) dt$$

where  $t'$  is the duration of the simulation. Figure 2(a) shows the moment current,  $p_x(t)$ , and the mean moment current,  $\bar{p}_x$  for a system where the angular pumping frequency is  $\omega = 2\pi/20$  and where the pumping mechanism is located at a point of asymmetry  $x = 0.75L_x$ . As it can be seen, the momentum current is oscillating, however, the mean momentum current tends to some non-zero value meaning that there exists a uni-directional mean flow in the system. The power spectrum of the moment current reveals that the signal is dominated by one frequency which is simply  $\omega/2\pi$ .

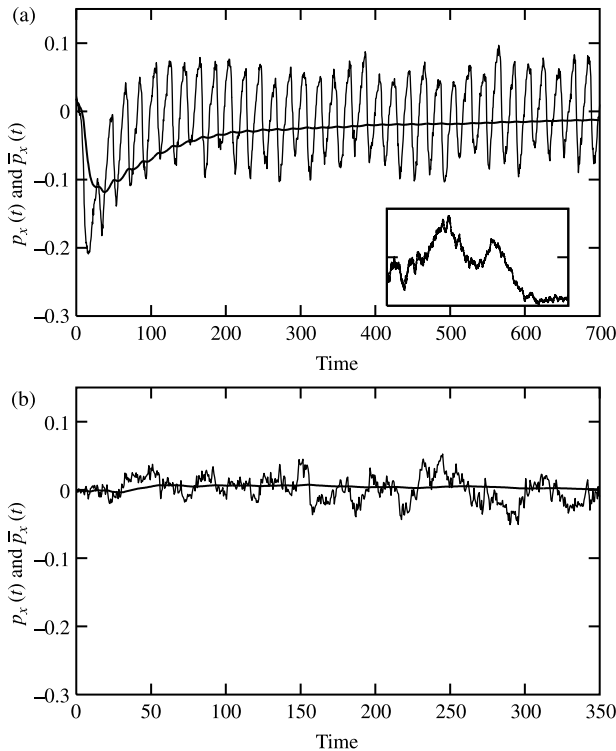


Figure 2.  $p_x(t)$  (thin line) and  $\bar{p}_x$  (thick line) vs time for  $\omega = 2\pi/20$ . (a) Pumping device located at point of asymmetry. The superimposed figure shows the mean moment current for  $t \in [5000, 15000]$ . (b) Pumping device located at the point of symmetry.

The superimposed figure is the mean moment current for the last 500 pumping cycles. It is seen that  $\bar{p}_x(t)$  fluctuates but remains non-zero. Figure 2(b) gives the results obtained after the pumping device is moved to the middle of the wider channel, i.e. to a point of symmetry. As expected,  $\bar{p}_x$  vanishes within the statistical error in agreement experimental results [5].

In [5] it is reported that the direction of the mean flow changes many times as the pumping frequency varies. To see whether this can be reproduced by molecular dynamics simulations the mean moment current is computed for various pumping frequencies ranging from  $2\pi/100$  to  $2\pi/15$ . The results are summarised in figure 3. The direction of the mean flow does change, however, in the frequency range we were able to study using NEMD we observe only one directional change. Simulations of smaller angular frequencies always show a positive mean flow. For large  $\omega$  the pumping mechanism leaves the pumping area unoccupied by the fluid which results in high density away from the pumping area and no mean flow. As shown in figure 4, the flow direction can also be changed by varying the location of the pumping mechanism.

Since the flow exhibits oscillatory behavior we will characterise it through the Stokes parameter  $\Lambda = r_0/\delta$ ,

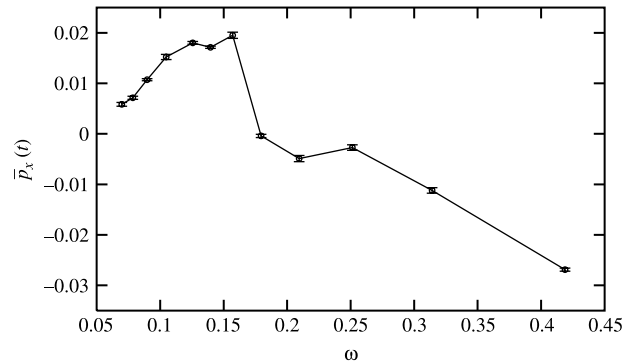


Figure 3. Mean momentum current vs pumping frequency. The error bars represent the standard deviation for the last 500 pumping cycles.

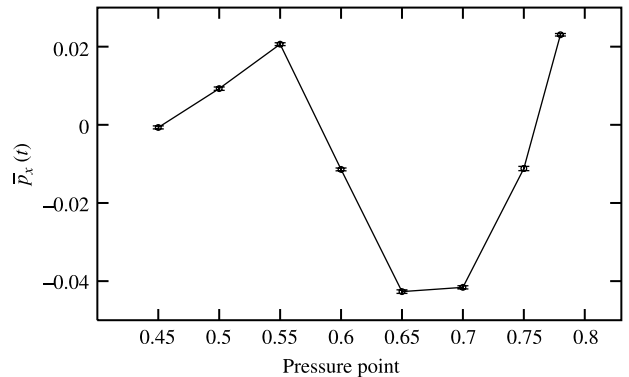


Figure 4. Mean momentum current vs the location of the pump given as fraction of tube length. The pumping frequency is  $2\pi/20$ . The error bars are the same as in figure 3.

where  $\delta = \sqrt{2\nu/\omega}$  is the Stokes layer with  $\nu$  denoting the kinematic viscosity and  $r_0$  is the radius of the wider channel. Using NEMD to simulate a simple Poiseuille flow we have found that  $\nu \approx 2.02$  (with a residual standard deviation of  $1.5 \times 10^{-4}$ ), see [21,22] for details. We thereby obtain  $\Lambda = 2.81$  which is about nine times smaller than in the experiments [5]. It is generally agreed that instabilities are located in the Stokes boundary layer. If the boundary layer is sufficiently small compared to the physical dimensions of the system it can cause a transition to turbulence, see [23] and references therein. To check whether such instabilities are likely to occur in the microscopic simulations we evaluate the Reynolds number based on the Stokes layer  $Re_\delta = u_0\delta/\nu$ , where  $u_0$  is the maximum amplitude of the stream velocity (which has the same value as the moment current in reduced units). We find that  $Re_\delta \approx 0$  which is in the same order of magnitude as the physical system. Now, in an oscillatory flow with zero mean instabilities are known to occur for  $Re_\delta > 100$  over a large range of the Stokes parameter [23]. Instabilities are consequently not expected here. It must be stressed that a global kinematic viscosity is not well defined in the microscopic NEMD since many of the physical parameters vary in both time and space. Nevertheless, even large variations of the kinematic viscosity does not considerably effect the values of the Reynolds number.

Focusing on the spatio-temporal variation of the fluid properties, we define the local density,  $\rho$ , the translational kinetic energy,  $E$  and the stream velocity,  $\mathbf{u}$ , from the microscopic quantities according to [15,8]:

$$\rho(\mathbf{r}, t) = \sum_i^N m_i \delta(\mathbf{r} - \mathbf{r}_i(t)) \quad (2)$$

$$E(\mathbf{r}, t) = \frac{1}{\rho(\mathbf{r}, t)} \sum_i^N m_i \mathbf{v}_i^2 \delta(\mathbf{r} - \mathbf{r}_i(t)) \quad (3)$$

$$\mathbf{u}(\mathbf{r}, t) = \frac{1}{\rho(\mathbf{r}, t)} \sum_i^N m_i \mathbf{v}_i \delta(\mathbf{r} - \mathbf{r}_i(t)) \quad (4)$$

Here,  $\delta(\mathbf{r} - \mathbf{r}_i(t))$  is the Dirac delta function. In practise the delta function is replaced by a step function which evaluates to 1 if fluid particle  $i$  is located in the sub-domain associated with a given area and zero otherwise. We determine the quantities given in equations (2)–(4) in the  $y$ -direction in a slab of dimensions  $0.1L_x \times L_y$  with  $0.2L_x \leq x \leq 0.3L_x$ . In the  $x$ -direction parallel to the mean flow the stream velocity is written as:

$$u_x(y, t) = \frac{1}{0.1L_x} \int_{0.2L_x}^{0.3L_x} u_x(\mathbf{r}, t) dx \quad (5)$$

where  $y \in [-r_0; r_0]$ , and so forth for the energy and density. In order to decrease the noise to signal ratio we divide the period of the pumping into 8 equally sized time

intervals and make sample averages over each interval. Since the moment current shows regular oscillations we make averages over all cycles as well. Figure 5 shows the density, the translational kinetic energy and the stream velocity.

First, we notice large spatial inhomogeneities near the wall–fluid boundary. These microscopic structures do not differ from the corresponding equilibrium situation, steady laminar flows (e.g. Poiseuille flows) or oscillatory flows with zero mean and they only result in spatial variations of the transport coefficients if the channel width is very small (less than 6 molecular diameters) [7,9,10,21,24,25]. The observed temporal variation is due to the reduced volume generated by the pump. This leads to oscillatory structural changes (see superimposed figure) in the fluid as well as considerable

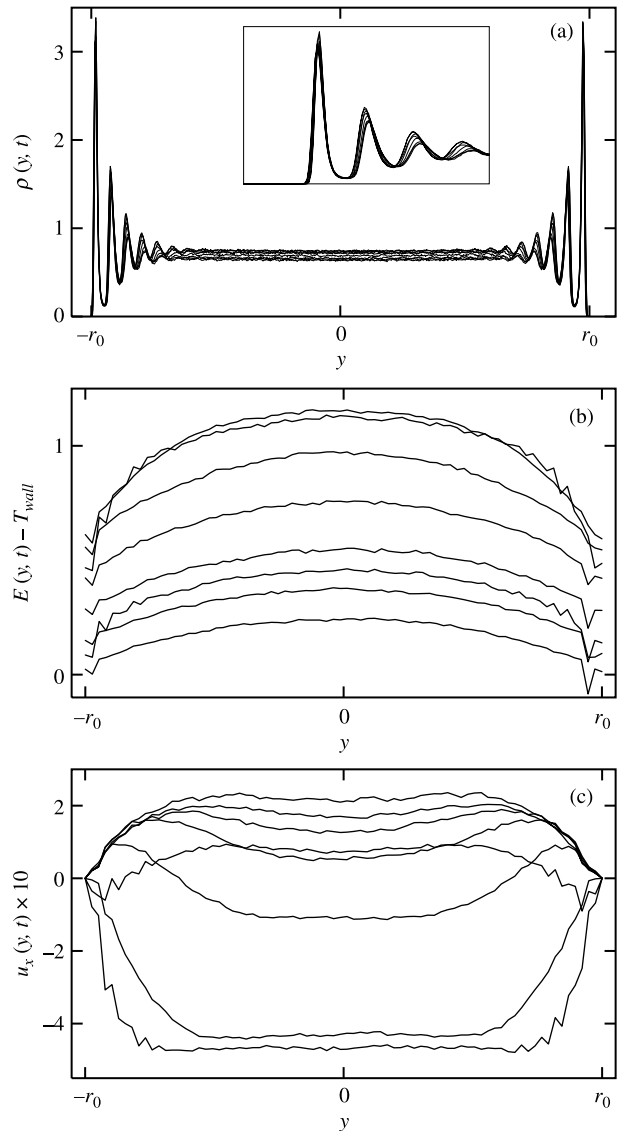


Figure 5. Spatio-temporal variations of: (a) density; (b) stream velocity in the  $x$ -direction,  $u_x$  and (c) translational kinetic energy. The data have been collected in the slab  $0.2L_x < 0.3L_x$ ,  $\omega = 2\pi/20$ . In 5(a) the superimposed figure shows the fluid structure near the wall fluid boundary.



variation in the transport coefficients. Using NEMD simulations of Poiseuille flow it we estimate that the kinematic viscosity varies up to 58% during a pressure cycle due to density variation. This in turn means on a microscopic scale the system exhibits rather large oscillations in the Stokes layer, namely, around 25% and the values discussed above are therefore average values. As already mentioned we do not expect any further instabilities due to the very low Reynolds number. This result is specific to the system considered where the pumping area is relatively large compared to the total area system. If the system is sufficiently large, we, therefore, argue that  $\rho$  follows the characteristics of the corresponding equilibrium situation if the system is sufficiently large.

Figure 5(b) shows that the translational kinetic energy (or temperature) exhibits very large temporal changes. Nevertheless, in the density range studied here the kinematic viscosity shows a very weak of temperature dependence of 1% which is lower than the statistical error.

The velocity profiles are depicted in figure 5(c). The fluid flows in the positive direction for most of the pressure cycle then abruptly changes direction moving in the opposite direction. As indicated by the temperature and density profiles this directional change is associated with a pressure increase and consequently a viscosity increase. This results in a decrease in the Stokes parameter. Nevertheless, the inertia forces relative to the viscous forces are still dominating due to the flow speed. Consequently, the Reynolds number is relatively large and we observe the plugged flow. As the flow speed decreases the viscous forces relative to the inertia forces are increasing which is manifested in “variable hat” profiles characteristic of a zero-mean oscillatory flow with relatively small Stokes parameter. During a pumping period, the dynamics can therefore be divided into an inertia dominated regime characterised by a plugged flow and a viscous dominated regime characterized by an oscillatory flow. In between these two regimes the flow is believed to be a superposition of the two.

#### 4. Model for the local stream velocity

The above discussion suggests the following empirical model for the  $x$ -component of the stream velocity:

$$u_x(y, t) = f_1(t)u_x^p(y, t) + f_2(t)u_x^o(y, t) \quad (6)$$

where  $u_x^p(y, t)$  and  $u_x^o(y, t)$  are spatio-temporal stream velocities for plugged flow and zero-mean oscillatory flow, respectively,  $f_1(t)$  and  $f_2(t)$  are weighting functions. We assume that  $f_1(t) + f_2(t) = 1$  for all  $t$ ,  $f_x \in [0; 1]$ ,  $n = 1, 2$  and that  $f_x(t)$  is oscillating in time with the same angular frequency,  $\omega$ , as the pumping device. We therefore choose the following functional expressions for the

weighting functions:

$$f_1(t) = \sin^2(\omega t) \quad \text{and} \quad f_2(t) = 1 - \sin^2(\omega t). \quad (7)$$

In this way, the flow has two extremes, namely, one extreme for relatively high Reynolds numbers where the flow is described fully by a plugged flow and one extreme for relatively low Reynolds numbers where it is given by a zero-mean oscillatory flow. Between these two extremes the flow is a superposition of the two. A zero-mean oscillatory flow with a pressure amplitude  $P$  is in complex notation given by [26]:

$$u_x^o(y, t) = \frac{P}{i\omega\rho} \left[ 1 - \frac{\cosh\left(\frac{1}{r_0}\Lambda + i\Lambda\right)y}{\cosh(\Lambda + i\Lambda)} \right] e^{i\omega t}. \quad (8)$$

Following [5] a plugged flow is assumed to be of the form:

$$u_x^p(y, t) = \frac{\gamma + 2}{\gamma} \left[ 1 - \left( \frac{y}{r_0} \right)^\gamma \right] \bar{u}_x^p(t) \quad (9)$$

where the parameter  $\gamma$  controls the flatness of the profile and where:

$$\bar{u}_x^p(t) = \frac{1}{2r_0} \int_{-r_0}^{r_0} u_x^p(y, t) dy. \quad (10)$$

We assume that the plugged flow is temporal oscillatory with the same frequency as the pumping device, with amplitude  $u_0$  and with a mean  $\bar{u}_x$ . Thus, we look for solutions of the integral equations given in equations (9) and (10) obeying:

$$\bar{u}_x^p(t) = u_0 \sin(\omega t) + \bar{u}_x \quad (11)$$

where

$$\bar{u}_x = \frac{1}{2tr_0} \int_0^{2\pi} \int_{-r_0}^{r_0} u_x(y, t) dy dt \quad (12)$$

a quantity deduced from the molecular dynamics simulations. Substituting equations (7)–(12) into equation (6) we obtain the following expression for the local stream velocity profile:

$$\begin{aligned} u_x(y, t) = & \frac{P}{i\omega\rho} \left[ 1 - \frac{\cosh\left(\frac{1}{r_0}(\Lambda + i\Lambda)\right)}{\cosh(\Lambda + i\Lambda)} \right] e^{i\omega t} \sin^2(\omega t) \\ & + \frac{\gamma + 2}{\gamma} \left[ 1 - \left( \frac{y}{r_0} \right)^\gamma \right] (u_0 \sin(\omega t) \\ & + \bar{u}_x \cos^2(\omega t)). \end{aligned} \quad (13)$$

The physical solution is then simply the real part of equation (13). In the following we use the physical parameters found in the molecular dynamics simulations, i.e.  $\Lambda = 2.81$ ,  $u_0 = 0.325$ ,  $r_0 = 15.5$ ,  $\bar{u}_x = -0.015$  and  $\rho = 0.6$ . The parameter  $\gamma$  is set to 10 throughout, leaving only the pressure amplitude  $P$  as a fitting parameter. Figure 6 shows eight velocity profiles for different times.

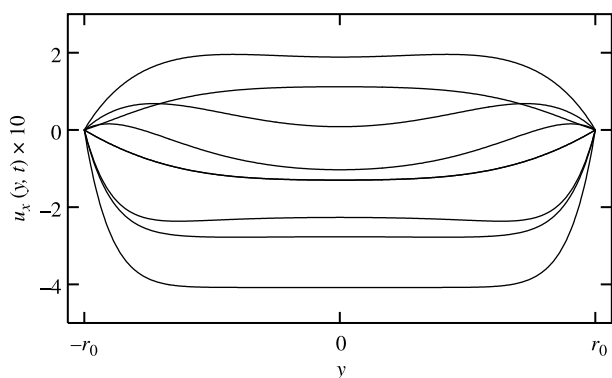


Figure 6. Velocity profiles as predicted by the model in equation (13).

As it can be seen the qualitative features of the dynamics are captured, i.e. the flow exhibit a plugged flow character as well as a zero-mean oscillatory flow dynamics. However, equation (13) does not show the same abrupt directional changes as the simulations. This may be because the flow in the microscopic simulations is not fully developed and due to the local variations in transport coefficients. A quantitative comparison between molecular dynamics and the model could be performed by including the local variations in the model, in particular in the expression of the Stokes parameter.

The local temporal dynamics can be investigated by integrating with respect to  $y$ :

$$\bar{u}_x(t) = \frac{1}{2r_0} \int_{-r_0}^{r_0} u_x(y, t) dy. \quad (14)$$

Figure 7(a) compares the values of  $\bar{u}_x(t)$  obtained with molecular dynamics simulations and the results obtained from equation (13) for the model. It is clearly seen that the model predicts a less abrupt increase of  $\bar{u}_x(t)$ , but the power spectrum given in figure 7(b) clearly reveals that the signal is composed of the main frequency  $\omega/2\pi$  as well as a higher frequency component in agreement with molecular dynamics. A third frequency is associated with a small amplitude is present in the molecular dynamics simulation. The comparison of power spectra deduced from the model and the molecular dynamics simulations proves that the empirical model for the local velocities captures the main dynamical features of the system. Note however, that the model is local and the study of different sections of the system requires changing the Stokes parameter.

## 5. Conclusion and perspectives

We have shown that the pumping mechanism suggested by Ottesen [5] can be successfully applied on very small time and length scales, and that, the system can be studied using NEMD. We have used the results obtained in the molecular dynamics to propose an empirical model for the local stream velocity, namely, a model that is a superposition of a plug flow and a zero-mean

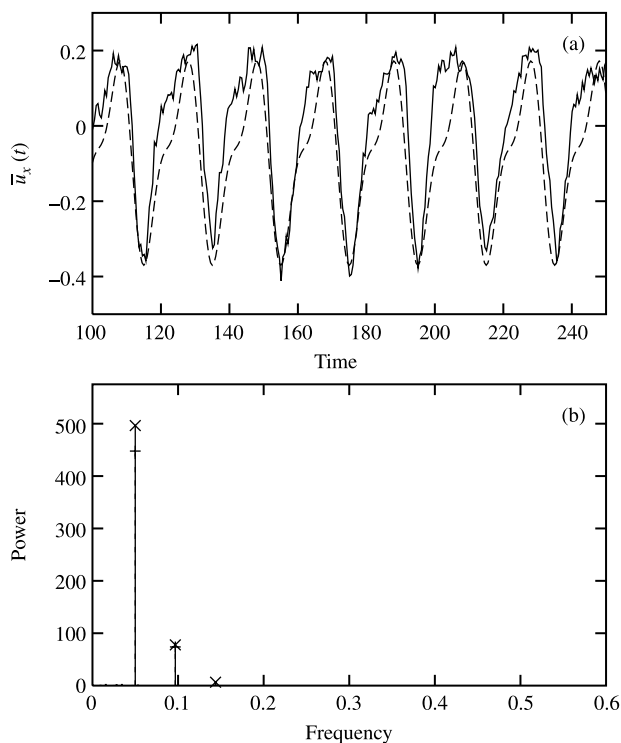


Figure 7. (a) Stream velocities obtained by the molecular dynamics simulations (full lines) and for the empirical model (dashed lines). (b) The corresponding power spectra, where + is the results from the molecular dynamics simulations and  $\times$  is from the model.

oscillatory flow. This model features two frequency components in the temporal variations of the stream velocity which are also found in the molecular dynamics simulations. However, the power spectrum of the model does not capture a third frequency of very small amplitude and the model does not predict the very abrupt change in flow. We argue that this may be because the flow is not fully developed in microscopic simulations and because the model does not take into account the variation of viscosity.

Instead of moving the walls, we have implemented the pump mechanism by applying an oscillatory pressure gradient in the pumping area. We have observed that this does not change the overall dynamical features in any way. In particular, we still observe the directional change of the flow. The original work done by Ottesen was concerned with modeling the cardio-vascular system, and the two rubber tubes had different elasticity. In the present simulations the two tubes have the same physical properties including same elasticity, because they are made of identical atoms with identical interaction potentials. In both systems the directional change is observed, indicating that this is independent of the details of the physical properties of the tubes.

We have here focused on a two dimensional system. It is debated whether the transport coefficients are well defined in two dimensions, because of the algebraic decay of the autocorrelation functions [27]. Nevertheless, many physical phenomena are observable in both two and three

dimensions, e.g. the characteristic quadratic velocity profile in a Poiseuille flow [22]. We, therefore, believe that the present simulations capture the true fluid dynamics. However, a more detailed study will include the third spatial dimension as well as a more realistic model for the wall, for example, by simulating valveless pumping in a carbon nanotube [13,14].

The pumping mechanism can be applied in various situations and molecular dynamics can in our opinion play an important role in predicting its applicability. For example, the work can be extended to very viscous fluids like polymers melts, or to charges particles.

## References

- [1] N-T. Nguyen, X. Huang. Miniature valveless pumps based on printed circuit board technique. *Sens Actuators, A*, **88**, 104 (2000).
- [2] J. Ouellette. A new wave of microfluidic devices. *Ind. Phys.*, (2003) Aug./Sept.
- [3] J.C.T. Eijkel, A. Van Den Berg. Nanofluidics: what is it and what can we expect from it? *Microfluidics Nanofluidics*, **1**, 246 (2005).
- [4] P. Woias. Micropumps—summarising the first two decades, In Proc. of SPIE. *Microfluidics BioMEMS* (2001).
- [5] J.T. Ottesen. Valveless pumping in a closed fluid-filled elastic tube-system; one-dimensional theory with experimental validation. *J. Math. Biol.*, **46** (2003).
- [6] J.T. Ottesen. Symmetric compressions of a fluid-filled torus of asymmetric elasticity generates mean flow of frequency dependent size and orientation, MIRIAM's in proceedings, in print
- [7] I. Bitsanis, T.K. Vanderlick, M. Tirrell, H.T. Davis. Tractable molecular theory of flow in strongly inhomogeneous fluids. *J. Chem. Phys.*, **89**, 13152 (1988).
- [8] K.P. Travis, B.P. Todd, D.J. Evans. Departure from Navier–Stokes hydrodynamics in confined liquids. *Phys. Rev. E*, **55**, 4288 (1997).
- [9] K.P. Travis, K.E. Gubbins. Poiseuille flow in Lennard–Jones fluids in narrow slit pores. *J. Chem. Phys.*, **112**, 1984 (2000).
- [10] J.S. Hansen, J.T. Ottesen. Molecular dynamics simulations of oscillatory flows in microfluidic channels, Submitted to *Microfluidics and Nanofluidics*
- [11] J. Castillo-Tejas, J.F.J. Alvarado, G. Gonzales-Alatorre, G. Luna-Barcenas, I.C. Sanchez, R. Macias-Salinas, O. Manero. Nonequilibrium molecular dynamics of the rheological and structural properties of the linear and branched molecules. Simple shear and Poiseuille flows; instabilities and slip. *J. Chem. Phys.*, **123**, 54907 (2005).
- [12] J. Delhommelle, D.J. Evans. Configurational temperature profile in confined fluids I. Atomic fluid. *J. Chem. Phys.*, **114**, 6229
- [13] J. Delhommelle, D. J. Evans. Configurational temperature profile in confined fluids II. Molecular fluid. *J. Chem. Phys.* **114**, 6236 (2001) (2001).
- [14] V.P. Stokhan, D. Nicholson, N. Quirke. Fluid flow in nanopores: an examination of hydrodynamic boundary conditions. *J. Chem. Phys.*, **115**, 3878 (2001).
- [15] V.P. Stokhan, D. Nicholson, N. Quirke. Fluid flow in nanopores: accurate boundary conditions for carbon nanotubes. *J. Chem. Phys.*, **117**, 8531 (2002).
- [16] D.A. McQuarrie. *Statistical Mechanics*, Harper & Row, New York (1976).
- [17] D. Rapaport. *The Art of Molecular Dynamics Simulation*, Cambridge University Press, Cambridge (1995).
- [18] S.J. Kim, H.I. Kim, S.J. Park, I.Y. Kim, S.H. Lee, T.S. Lee, S.I. Kim. Behavior in electric fields of smart hydrogels with potential application as bio-inspired actuators. *Smart Mater. Struct.*, **14**, 511 (2005).
- [19] S. Nosé. A unified formulation of the constant temperature molecular dynamics methods. *J. Chem. Phys.*, **81**, 511 (1984).
- [20] W.G. Hoover. Canonical dynamics: equilibrium phase–space distributions. *Phys. Rev. A*, **31**, 1695 (1985).
- [21] D. Frenkel, B. Smit. *Understanding Molecular Simulation*, Academic Press, San Diego (1996).
- [22] W.T. Ashurst, W.G. Hoover. Dense-fluid shear viscosity via nonequilibrium molecular dynamics. *Phys. Rev.*, **A11**, 658 (1975).
- [23] J. Koplik, J.R. Banavar, J.F. Willemsen. Molecular dynamics of fluid flow at solid surfaces. *Phys. Fluids*, **A1**, 781.
- [24] J.A. Cosgrove, J.M. Buick, S.J. Tonge. Evolution of turbulence in an oscillatory flow in a smooth-walled channel: a viscous secondary instability mechanism. *Phys. Rev.*, **E68**, 26302 (2003).
- [25] F.F. Abraham. The interfacial density profile of a Lennard–Jones fluid in contact with a (100) Lennard–Jones wall and its relationship to idealized fluid/wall systems: a Monte Carlo simulation. *J. Phys. Chem.*, **68**, 3713.
- [26] S.T. Cui. Molecular self-diffusion in nanoscale cylindrical pores and Fick's law predictions. *J. Chem. Phys.*, **123**, 54706 (2005).
- [27] F.A. Englund. *Hydrodynamik—Newton'ske vædskers mekanik*, Danmarks tekniske højskole, Lyngby (1968).
- [28] M.A. van der Hoef, D. Frenkel. Evidence for faster-than- $t^{-1}$  decay of the velocity autocorrelation function in a 2D fluid. *Phys. Rev. Lett.*, **66**, 1591 (1991).